CO_2 hydrogenation to methanol with Ga- and Zn-doped mesoporous Cu/SiO_2 catalysts prepared by the aerosol-assisted sol-gel process

Charlie Paris,[a,#] Dr Alejandro Karelovic,[b,*] Raydel Manrique,[b] Dr Solène Le Bras,[a] Dr François Devred,[a] Dr Vit Vykoukal,[c] Dr Ales Styskalik,[c,d] Pierre Eloy,[a] Prof Damien P. Debecker[a]*

[a] Institute of Condensed Matter and Nanoscience (IMCN), Université catholique de Louvain (UCLouvain), Place Louis Pasteur, 1, box L4.01.09, 1348 Louvain-La-Neuve, Belgium.

[b] Carbon and Catalysis (CarboCat), Department of Chemical Engineering, Faculty of Engineering, University of Concepcion, Chile.

[c] Masaryk University, Department of Chemistry, Kotlarska 2, CZ-61137 Brno, Czech Republic

[d] Masaryk University, CEITEC MU, Kamenice 5, CZ-62500 Brno, Czech Republic

* corresponding authors: akarelov@udec.cl, damien.debecker@uclouvain.be

[#] currently at Cardiff Catalysis Institute (CCI), School of Chemistry, Cardiff University, Main Building, Park Place, Cardiff, CF10 3AT, UK. E-mail: pariscb@cardiff.ac.uk

Abstract

The preparation of copper-based heterogeneous catalysts dedicated to the hydrogenation of CO_2 to methanol typically relies on multi-step procedures carried out in batch. These steps are precisely tailored to introduce the active phase (Cu) and the promoters (e.g. zinc, gallium) onto a preformed support, to maximize catalyst performance. However, each process step – often carried out in batch – can be associated with the formation of waste and with the consumption of energy, thereby negatively impacting the environmental performance of the overall catalyst preparation procedure. Here, we propose a direct and continuous production process for the synthesis of efficient catalysts for the CO_2 to methanol reaction. Gallium- and zinc-promoted mesoporous Cu-SiO_2 catalysts are prepared in one step by the aerosol-assisted sol-gel process. The catalysts consist of spherical microparticles and feature high specific surface area and pore volume, with interconnected pores of about 6 nm. A strong promoting effect of Ga and Zn is highlighted, boosting the selectivity for methanol at the expense of CO. Upon calcination, we show that Cu species – initially trapped in the silica matrix – undergo a migration towards the catalyst surface and a progressive sintering. After optimization, the catalysts obtained via such direct, continuous, simple, and scalable route compete with the best catalysts reported in the literature and obtained via multi-step approaches.

Keywords

CO_2 hydrogenation, aerosol-assisted sol-gel process, copper catalyst, CH_3OH synthesis, mesoporous metallosilicate

Introduction

Anthropogenic emissions of CO_2 have a marked effect on the climate and on the environment.[1] Under the umbrella of the Paris agreement, the international community is largely committed to tackle this issue.[2] In a scenario where the production of renewable energy is boosted, it will be possible to produce "green hydrogen" at large scale (Power-to-Hydrogen scenario).[3] Concomitantly, CO_2 has to be captured from local emission points, purified and further converted by hydrogenation to methane, methanol, olefins, etc.[4] This so-called "power-to-X" scenario has attracted significant interest during the last decade.[5] Arguably, the development of high-performance nanostructured heterogeneous catalysts is one of the main scientific key to unlock the potential of this strategy and important progress is currently being made in this field.[6]

As a platform molecule, methanol is a sustainable source of liquid fuels and one of the most useful organic chemicals.[7] Methanol finds many applications in the chemical industry and can be incorporated into the energy portfolio as an efficient storage system.[8] The current industrial production of methanol is primarily achieved from syngas (reaction 1) using Cu-based catalysts but methanol can also be produced directly by the hydrogenation of carbon dioxide (reaction 2).[9] Simple copper-based catalysts, however, are not suitable for the direct hydrogenation of CO_2 since they preferentially catalyse the reverse water-gas shift reaction (RWGS, reaction 3) under the typical process conditions (5-10 *MPa*; 200-300 °*C*).[9,10] The occurrence of the RWGS negatively impacts the selectivity of the CO_2-to-methanol process, and is also known to decrease the catalyst lifetime.[11] Therefore, modifications of the catalytic system are required to improve the performance, and this can be achieved using appropriate dopants.

(1) $CO + 2\ H_2 \rightarrow CH_3OH$; $\Delta H_{298K} = -90.8\ kJ\ mol^{-1}$

(2) $CO_2 + 3\ H_2 \rightarrow CH_3OH + H_2O$; $\Delta H_{298K} = -49.5\ kJ\ mol^{-1}$

(3) $CO_2 + H_2 \rightarrow CO + H_2O$; $\Delta H_{298K} = +41.2\ kJ\ mol^{-1}$

Catalysts dedicated to the CO_2-to-methanol reaction consist of supported Cu promoted by another metal (e.g. Zn, Ga, Ce, Zr).[12] Among them, Cu-ZnO systems are the most studied.[13] The synergetic effect on catalytic performances is usually explained by (i) the formation of surface defects,[14] (ii) the creation of active sites of CuZnO alloy, implying oxygen vacancies and $Cu^{\delta+}$ species,[15] or (iii) a hydrogen reservoir at the surface of the zinc oxide phase.[16] Gallium has been added as a promoter to Cu/ZnO, Cu/ZrO_2 or Cu/SiO_2

catalysts to form $Cu/ZnO/Ga_2O_3$,[17] $Cu/ZrO_2/Ga_2O_3$,[18] $Cu/ZnO/ZrO_2/Ga_2O_3$,[19] or $CuGa/SiO_2$.[20] The positive effect of Ga addition on catalytic activity for the direct hydrogenation of CO_2 towards methanol has been proposed to proceed via several possible phenomena. For $Cu/ZnO/Ga_2O_3$ catalysts, Schumann *et al.*[17a] proposed that Ga^{3+} species exert a direct structural promotion effect. On the other hand, Tsang and co-workers[17c] suggested that Ga^{3+} promotes the formation of highly active alloyed CuZn nanoparticles via a facilitated reduction of ZnO to Zn^0. Studies focused on $Cu/ZnO/ZrO_2/Ga_2O_3$ catalysts concluded that Ga_2O_3 increases the number of active sites by increasing the Cu dispersion.[19] Toyir et al. reported that the Cu^+:Cu^0 ratio is affected by the presence of Ga, impacting the performances of Cu/ZnO catalysts.[17b] In the same study, however, they reported no promotional effect of gallium on Cu/SiO_2 catalysts. Conversely, Medina *et al.*[20] have shown that gallium promotion increases the selectivity of Cu/SiO_2 catalysts towards methanol. Performing *in-situ* DRIFTS during CO_2 hydrogenation reaction at steady state, they observed no influence of the Ga presence on the oxidation state of Cu (mainly Cu^0) but an enhanced formation of formate adsorbates on Ga_2O_3 species. More recently, Copéret and co-workers prepared alloyed CuGa nanoparticles supported on SiO_2 using a surface organometallic chemistry technique.[21] They assigned the enhanced catalytic activity and selectivity towards methanol to an increased interfacial area between Ga_2O_3 and Cu^0, where methoxy intermediates are stabilized. While the precise mechanism of promotion continues to be debated, it should be kept in mind that the hydrogenation of CO_2 to methanol on Cu-based catalysts is strongly structure-sensitive.[22] In this regard, regardless of the catalyst preparation procedure, the Cu nanoparticles size is a key factor dictating performance. Also, for promoted catalysts, the interaction between the active Cu NP and the promoter is important.[23]

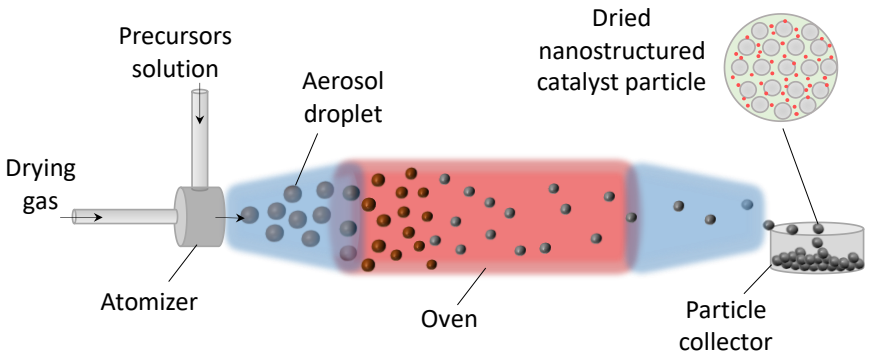
Thus, there is a dense body of literature covering all aspects of catalyst preparation, in a search for a fine control on particles size, on particle size distribution, on the interaction between the (promoted) support and the Cu NP, on catalyst textural properties, etc.[24] Conventional catalyst preparation procedure, however, systematically consist in multi-step batch procedures (co-precipitation, drying, calcination, impregnation of the promoter, calcination, impregnation of the active phase, calcination, reduction, etc.). Each step is usually carried out in batch mode and involves the utilization of energy or the production of waste. Such multi-steps batch procedures are considered to have low environmental performance an intensification of catalyst preparation procedure should be targeted.

Aerosol processes are currently emerging as promising synthesis routes to nanomaterials – especially heterogeneous catalysts[25] – and have a bright forecast in terms of sustainability.

Based on the atomization and fast drying of a precursors solution or suspension, this bottom-up technique allows the one-step and continuous production of nanomaterials with tailored composition, textural and surface properties.[26] One of the decisive advantages of the method is that it is can be operated in a continuous way. Thus, waste production and energy consumption is typically lower than with multi-step batch processes; moreover, the method is considered to be easily scalable.[26,27]

The aerosol-assisted sol-gel processes (AASG) can be defined as the combination of spray drying with sol-gel chemistry, and was already identified as a powerful means to prepare tailor-made heterogeneous catalysts.[28] Typically, a precursor solution is sprayed in the form of a mist of air-borne droplets using an aerosol generator, and the droplets are processes through a drying chamber where the volatile solvent is removed and where the sol-gel polycondensation reactions occur rapidly (Scheme 1). The dried particles are recovered in a collector (cyclone, filter, etc.). Playing on the atomization and/or drying conditions allows tuning the particles size, morphology, etc.[29] Leveraging on sacrificial pore-generating agents, the texture of the materials can be fine-tuned.[26,30] The versatility of sol-gel chemistry gives access to a wide range of materials. Interestingly, the rapid drying of the droplets allows forming solids in metastable states, including highly homogeneous metallosilicates which are of great interest in the field of heterogeneous catalysis.[28b] Recently, enhanced performance has been reported for catalysts prepared by such route in a range of applications: hydrocarbon isomerization,[31] lactate synthesis,[32] olefin metathesis,[33] selective oxidation of olefin,[30,34] carboxymethylation,[35] mild oxidation of sulphur compounds,[36] etc. The method was recently applied to synthesize noble metal-based catalysts with hierarchical structure showing record performance in electrocatalysis.[37] In the field of CO_2 hydrogenation, the AASG route has been successfully applied to synthesize mesoporous titania supports for Ru-based methanation catalysts.[38]

Herein, we propose to exploit AASG to prepare Cu-based catalysts dedicated to the conversion of CO_2 to methanol. Cu/SiO_2 catalysts consisting of spherical and mesoporous particles, promoted either by Zn or Ga, are obtained in one-pot, in a continuous way. We investigate the influence of the calcination temperature, as well as the nature of the promoter, on their catalytic performances. With this new catalyst production process in hand, we design efficient hydrogenation catalysts and we step forward in the understanding of the promotional effect of Zn and Ga.



Scheme 1. Schematic view of the AASG process that can be operated in a continuous mode for the one-pot production of nanostructured catalysts.[25] The precursor solution contains a solvent, metal precursors, and a templating agent (e.g. a surfactant that will form micelles via evaporation-induced self-assembly, EISA). The droplets formed by atomization are transported in a drying gas towards a drying zone where the formation of structured particles takes place.

Results and discussion

Mesoporous silica and Ga- or Zn-doped silica supports impregnated with Cu

Utilizing the aerosol-assisted process, we prepared a mesoporous silica material (Si-550) as a mesostructured support for Cu. This material consisted in spherical particles, with a diameter ranging from 0.1 to 5 μm (Figure S1). Their spherical shape originates from the fact that they are obtained through the drying of spherical aerosol droplets. As a result of the templating effect brought by the sacrificial surfactant used in the synthesis (evaporation-induced self-assembly of F127), the solid exhibited a mesoporous texture, with relatively large specific surface area, large pore volume and a pore size distribution centred on 5-6 *nm* (see below). Copper was loaded onto this support using a classical dry impregnation method to obtain DI-Cu/Si-550. This DI-Cu/Si-550 catalyst showed very poor activity in the hydrogenation of CO_2 to methanol (Figure 1). Not only the CO_2 conversion was very low, but also the MeOH selectivity remained as low as ~10% (the rest being converted to CO).

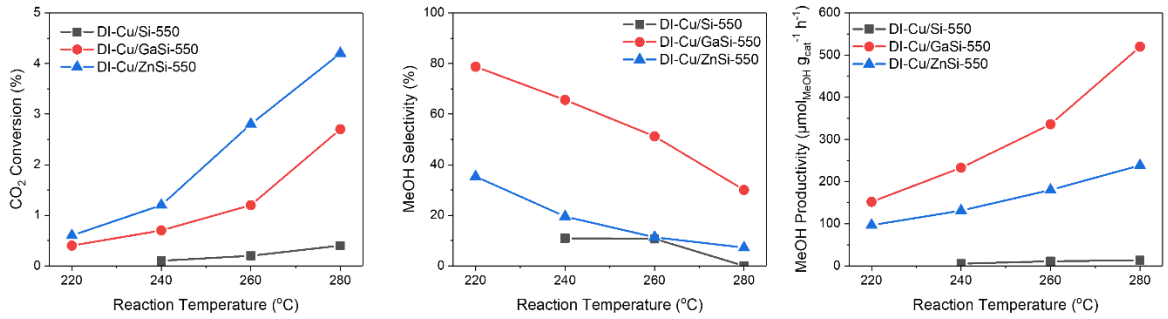


Figure 1. Catalytic hydrogenation of CO_2 with catalysts prepared by dry impregnation on Cu onto mesoporous supports. CO_2 conversion (left), MeOH selectivity (middle) and MeOH productivity (right).

It is known that the copper-catalysed conversion of CO_2 to MeOH is strongly promoted by Zn[39] and Ga.[20,21] Also, the dispersion of the promotor should be high to create high interfacial area between the promoter and the Cu nanoparticles.[20,40] Thus, exploiting the ability of the aerosol-assisted sol-gel process to produce highly homogeneous metallosilicates, we have prepared Ga- and Zn-promoted silica supports (GaSi-550 and ZnSi-550). The nominal molar ratio of promoter/Si was 0.05. Upon addition of Cu by dry impregnation, the promoted catalysts (DI-Cu/GaSi-550 and DI-Cu/ZnSi-550) showed much higher activity in the production of methanol as compared to the non-promoted DI-Cu/Si-550 catalyst (Figure 1). Both conversion and MeOH selectivity increased drastically, and the effect was more pronounced for the Ga-promoted catalysts. Rather than obtaining high conversion, or even high yield (or productivity), attaining high selectivity is important in the perspective of an industrial process, because it ensures a thorough use of the H_2 and it facilitates downstream purification.[41] Here, methanol selectivity was markedly promoted by the presence of the dopants. At 220 °*C*, the non-promoted catalyst is virtually inactive, but the Zn- and Ga-promoted catalysts reached 97 $\mu mol_{MeOH} g_{cat}^{-1} h^{-1}$ and 152 $\mu mol_{MeOH} g_{cat}^{-1} h^{-1}$, respectively. At this temperature, the Ga-promoted catalyst exhibited an outstanding MeOH selectivity of 79%. Increasing the reaction temperature provoked a progressive diminution in MeOH selectivity but markedly boosted conversion, resulting in an overall increase in methanol productivity (520 $\mu mol_{MeOH} g_{cat}^{-1} h^{-1}$ at 280 °*C*). Recent reports, using $CuGa/SiO_2$ catalysts prepared by reverse microemulsion technique attained only ca. 420 $\mu mol_{MeOH} g_{cat}^{-1} h^{-1}$ under the same reaction conditions.[20] The high activity showed by our catalysts might be related to a better dispersion of Ga species and hence a better contact with Cu nanoparticles.

From the data presented in Figure 1, the Arrhenius plots can be built to estimate the apparent activation energy (Figure S2 and Table S1). While the apparent activation energy for CO formation tended to increase upon promotion (76, 119, and 108 $kJ.mol^{-1}$ respectively for the un-promoted, Ga-promoted and Zn-promoted catalysts), the apparent activation energy for MeOH formation dropped upon promotion (56, 46, and 34 $kJ.mol^{-1}$ respectively for the un-promoted, Ga-promoted and Zn-promoted catalysts). Therefore, the promotion effect of Ga or Zn can be interpreted by the fact that the dopants favour the formation of new active sites with higher intrinsic activity (lower activation energy), and not simply by the fact that they would promote the formation of more numerous active sites of identical intrinsic activity. This is consistent with previously reported observations.[20,21]

Cu-based catalysts prepared in one-pot

Stepping further towards the sustainable production of effective hydrogenation catalysts, we propose the one-step preparation of promoted copper catalysts. In this case, the copper salt is simply incorporated in the precursors solution (already containing pre-hydrolysed TEOS, surfactant and dissolved promoter salt) right before spray drying. Avoiding the batch impregnation step, such a direct one-step process allows envisaging a catalyst production in a fully continuous mode.

In order to assess the reliability of such one-pot synthesis route, the catalyst composition was verified by ICP-AES (Table 1). The actual copper loading was systematically a bit lower than the targeted one (~8 *wt.%* instead of 10 *wt.%*). This may be due to the hygroscopic properties of the metal precursor, biasing the mass measurement owing to adsorbed moisture. Yet, the Cu loading was very consistent in all the preparations. Both promoters (Ga and Zn) were detected at the expected concentrations, corresponding to the targeted promoter/Si molar ratio (0.05). Overall, the one-pot aerosol route can be considered to offer a good control on bulk composition.

Table 1. Composition of one-pot aerosol-synthesized catalysts determined by ICP-AES.

Sample	Cu (*wt.%*)	Si (*wt.%*)	Zn or Ga (*wt.%*)	Zn/Si or Ga/Si (-)[a]
A-CuSi-550	7.7	36.2	-	-
A-CuZnSi-550	7.8	32.5	3.7	0.049
A-CuGaSi-550	8.0	34.3	4.0	0.047

[a] molar ratios

The morphology of Cu-based catalysts prepared by the one-pot method was typical of mesoporous metallosilicate obtained by AASG and was the same as that of the silica supports presented above. By (scanning) transmission electronic microscopy, one can clearly observe mesostructured spherical particles with mesopores down to the core of the particles (Figure 2). At relatively high magnification, on small particles, copper oxide nanoparticles of a few nanometers can be observed, as darker spots. This is confirmed by STEM-EDS, where the elemental mapping shows that Cu is dispersed homogeneously throughout the catalyst particles, in the form of nanoparticles of a few nanometre in size. For the Ga- and Zn-doped catalysts, the same mesostructures are observed and the formation of Cu nanoparticles appears similar (Figure S3 and S4). Importantly, the dopants (Ga or Zn) appear homogeneously dispersed throughout the microspheres.

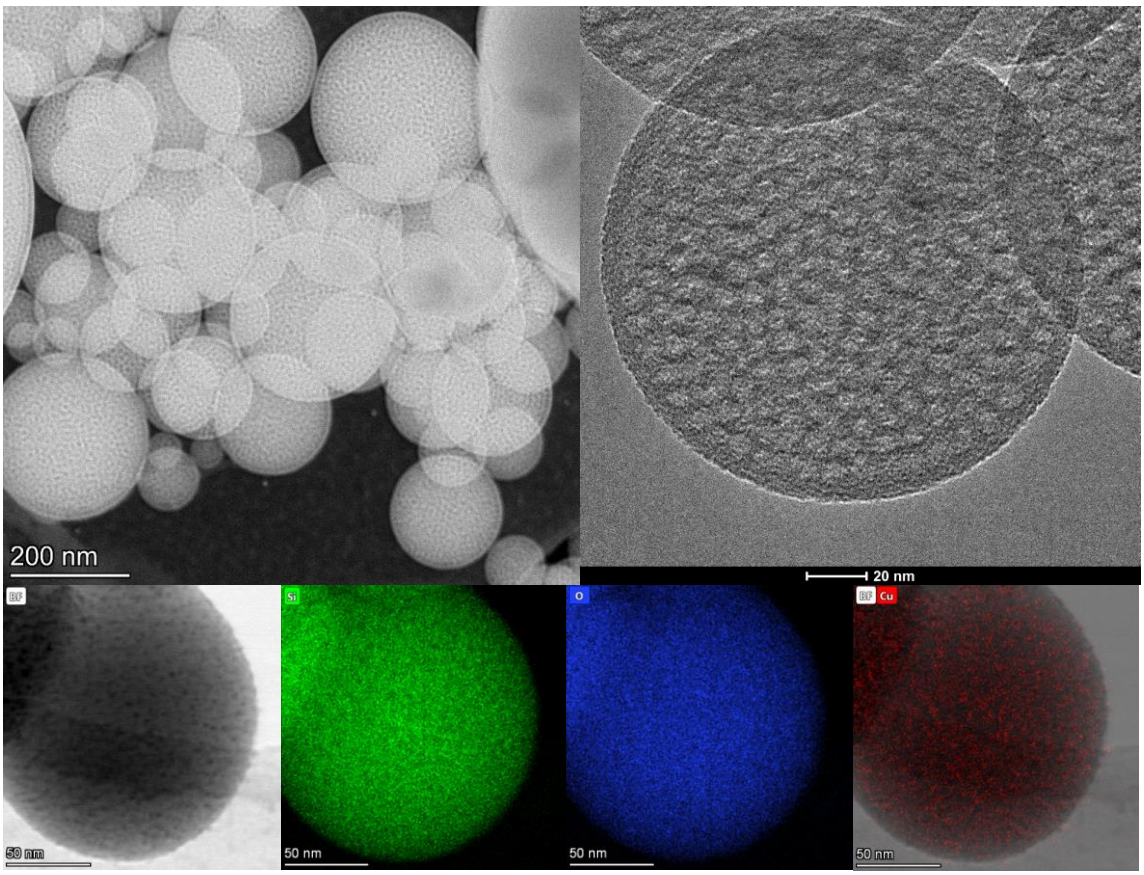


Figure 2. Electron micrographs of A-CuSi-550 observed in (top left) dark field STEM, (top right) TEM, and (bottom) STEM-EDS with elemental mapping of Si in green, O in blue, and Cu in red. A-SuGaSi-550 and A-CuZnSi-550 were very similar, with also a homogeneous dispersion of Ga and Zn (see supplementary information, Figure S3 and S4)

In nitrogen physisorption, the catalysts featured Type IV isotherms associated with the presence of open mesopores (Figure 3). The shape of the hysteresis loop corresponds to the H2-type (asymmetrical with a steeper desorption branch than the adsorption branch) characteristic of restrictions within the porous network. The forced closure of the hysteresis loop at p/p_0 values of 0.4-0.5 indicated the presence of mesopores smaller than 3.8 *nm*.[42] The BJH model applied on the adsorption branch of the isotherm revealed the presence of mesopores of about 5-6 *nm*, in line with TEM observations (Table 2). The steep nitrogen uptake at very low pressure indicated the presence of micropores as well, which however represents a minor contribution to the total pore volume. The specific surface area and pore volume were higher for promoted catalysts as compared to A-CuSi-550, reaching values as high as 430 m^2g^{-1} and 0.30 cm^3g^{-1} for A-CuGaSi-550.

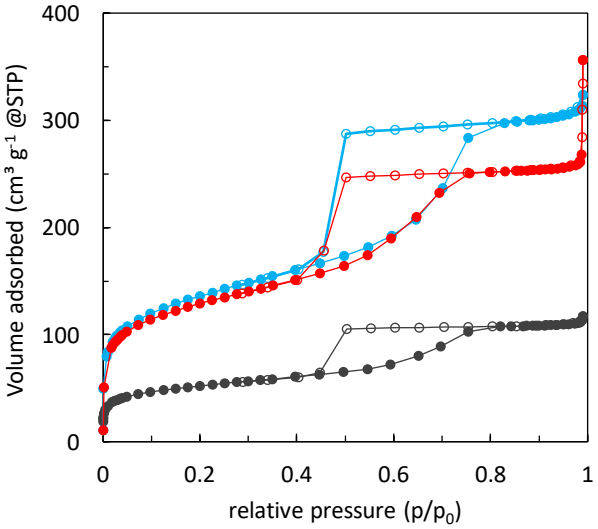


Figure 3. N_2 physisorption isotherms of catalysts prepared in one step via the AASG process and calcined at 550 °*C*. (black) A-CuSi-550, (blue) A-CuZnSi-550, (red) A-CuGaSi-550. Full symbols are used for the adsorption isotherms and empty symbols for desorption isotherms.

Table 2. Textural properties of catalysts prepared in one step via the AASG process.

Sample	**Surface Area** ($m^2.g^{-1}$)	**V_p** ($cm^3.g^{-1}$)	**V_{micro}** ($cm^3.g^{-1}$)	**D_p** (*nm*)
A-CuSi-550	180	0.13	0.03	5
A-CuZnSi-550	460	0.36	0.06	6
A-CuGaSi-350	510	0.33	0.09	5
A-CuGaSi-550	430	0.30	0.06	6
A-CuGaSi-650	290	0.25	0.05	5
A-CuGaSi-750	70	0.01	0.001	-

In the hydrogenation of CO_2 to MeOH (Figure 4), A-CuSi-550 was about one order of magnitude more active than the corresponding catalyst prepared by impregnation, but MeOH selectivity remained poor. As a result, the MeOH productivity was very low. With the promoted catalysts, however, a strong positive effect on MeOH selectivity was again highlighted. This was particularly true for the Ga-promoted catalyst, which reached a record MeOH selectivity of 85 % at 220 °C. Conversion was modified positively for Zn, and negatively for Ga. Overall, the Ga-promoted catalyst (A-CuGaSi-550) was the most productive catalyst. For this catalyst, a marked decrease in the activation energy for the formation of MeOH was calculated (27 $kJ.mol^{-1}$, see Table S1 and Figure S2). Nevertheless, it performed somewhat lower that the corresponding catalyst prepared by impregnation of Cu onto GaSi-550, probably owing to a lower amount of active sites available at the surface.

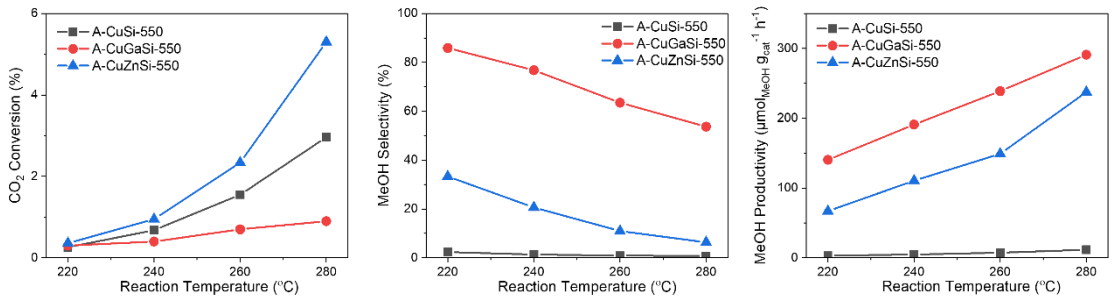


Figure 4. Catalytic hydrogenation of CO_2 with catalysts prepared by the one-pot aerosol-assisted sol-gel method. CO_2 conversion (left), MeOH selectivity (middle) and MeOH productivity (right).

With such one-pot preparation approach, calcination plays a crucial role. Indeed, the AASG process is expected to lead to the dispersion of Cu *into* (and not necessarily *onto*) the metallosilicate matrix, because the process is known to favour a so-called "kinetic quenching" of the sol-gel reactions, which typically results in the formation of solids with a homogeneous composition.[25] This can be expected to promote a more intimate interaction between the Cu species and the (promoted) silica matrix. Yet, it was not evident that active Cu nanoparticles could be formed, and that the latter would be available at the surface of the materials to act in the catalytic reaction.

In fact, XRD showed that the freshly prepared A-CuSi material (before calcination) was totally amorphous (Figure 5). This is consistent with the formation of a material with copper species homogeneously dispersed in the metallosilicate matrix. Upon calcination at 350 °C, the

onset of CuO diffraction peaks was observed (2θ = 35.5°, 38.7° and 48.8°).[43] Using in situ XRD, we followed the evolution of the sample crystallinity upon increasing temperature. CuO diffraction peaks progressively shifted to smaller angles due to the thermal dilatation of the sample. More importantly, the CuO diffraction peaks became more intense and narrower as the calcination temperature increased, indicating the progressive formation of larger CuO nanoparticles. Calculations of the CuO nanoparticles size via the Scherrer equation showed that the estimated size progressively grew from 11 *nm* for the catalyst calcined at 350 °*C* to 37 *nm* for the catalyst calcined at 750 °*C* (Figure S5).

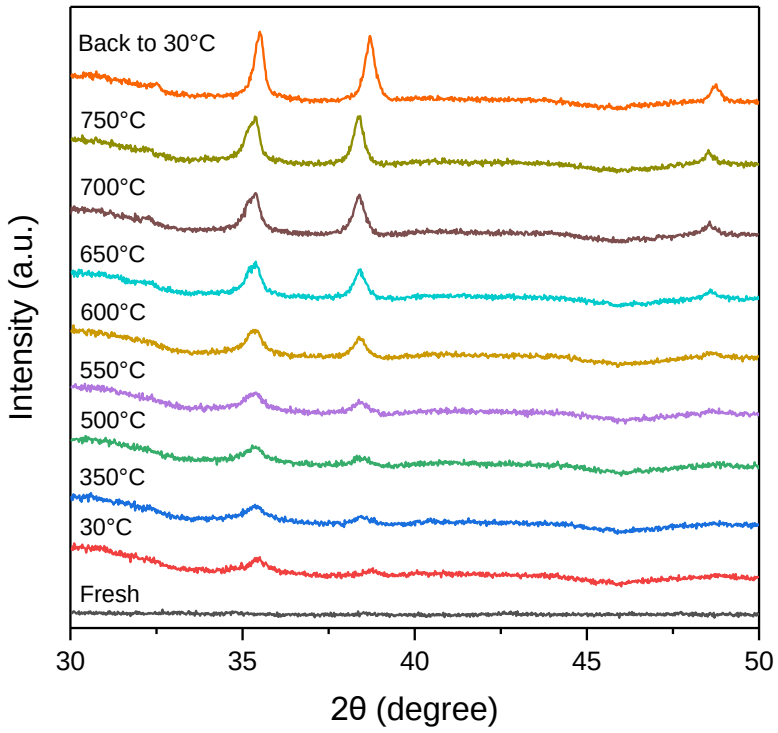


Figure 5. *In-situ* X-Ray diffractograms of A-CuSi. The grey line corresponds to the fresh powder obtained directly from the aerosol process. The other diffractograms come from the same catalyst which has undergone the first calcination step *ex situ*, at 350 °*C* and is brought to the indicated temperature (from 30 °*C* to 750 °*C* and back to 30 °*C*) in the XRD apparatus (in air).

The best catalytic formulation (A-CuGaSi) has been subjected to different calcination temperatures. Increasing the calcination temperature from 350 °*C* to 650 °*C* resulted in a moderate reduction of the specific surface area and pore volume (Table 1). The mean pore diameter stayed constant (5-6 *nm*). However, at 750 °*C*, the mesostructure was lost and the specific surface area and pore volume dropped dramatically. XPS analyses showed that the dispersion of Ga oxide species remained relatively unaffected by the different thermal

treatments (except 750 °*C*) (Table 2). On the contrary, the copper surface concentration increased noticeably with increasing calcination temperature (from 1.0 to 2.4 *at.%* when calcined at 350 °*C* to 750 °*C*). This indicated that the surface was progressively enriched in Cu when the calcination temperature was increased. At 550 °*C*, the Cu surface concentration was at the same level (~1.5 *at.%*) regardless of the presence of the promoter. After calcination at 650 °*C*, the Cu surface concentration was at the same level as what is observed for the impregnated catalyst.

Table 2 Surface composition as measured by XPS.

Sample	**Atomic concentration (%)**				
	Cu[a]	**O**	**Si**	**Ga or Zn**	**Ga/Si (-)**
A-CuSi-550	1.5	65.3	33.2	-	-
A-CuGaSi-350	1.0	61.2	32.7	5.1	0.16
A-CuGaSi-550	1.4	63.2	30.8	4.6	0.15
A-CuGaSi-650	1.8	62.7	30.9	4.7	0.15
A-CuGaSi-750	2.4	68.7	23.7	5.6	0.24
DI-Cu/GaSi-550	1.9	62.4	30.6	5.1	0.17

[a] Note that, from the observation of a broadening of the Cu $2p_{3/2}$ photoelectron peak, one may tentatively pinpoint the interaction between Cu and Ga species in the catalysts prepared in one pot by AASG when the calcination was done at 550 °*C* or 650 °*C* (see Figure S6).

Using N_2O chemisorption, we measured the Cu dispersion and found that it increased when the calcination temperature increases: from 6 *%* at 350 °*C* to 27 *%* at 550 °*C* and 31 *%* at 650 °*C*. This is not incompatible with a progressive sintering, as the latter is compensated by the migration towards the surface where copper can be titrated. For A-CuGaSi-750, however, the TCD signal in the N_2O chemisorption experiment was below the accuracy limit, suggesting that in this case, even if copper is present at the surface of the catalyst, its heavy sintering (see XRD) results in a very low dispersion.

Based on *in situ* XRD, XPS, and N_2O chemisorption results, we propose that calcination did not only provoke the elimination of the surfactant to release the mesoporosity but also modified the distribution of copper (Figure 6). XPS unambiguously showed that, even if Cu is first mostly dispersed into the metallosilicate matrix after the one-step AASG process, Cu species tend to migrate towards the catalyst surface under the effect of temperature. The driving force for this migration is the poor solubility of the Cu species into silica. In parallel, CuO nanoparticles are formed and progressively grow in size by sintering.

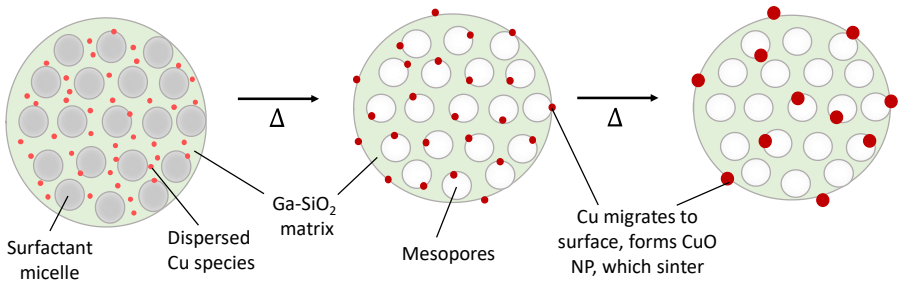


Figure 6. Schematic view of the mechanism that takes place during calcination of the catalysts prepared by AASG.

Consistent with the characterization data, the catalytic performance of this catalyst series showed that a too low or too high calcination temperature led to virtually inactive catalysts (Figure 7). After calcination at 350 °*C*, Cu is still mainly trapped in the walls of the porous Ga-SiO_2 material and not accessible for the catalytic reaction at the surface. It is also possible that the Cu nanoparticles are too small, as it is known that Cu-based hydrogenation catalysts are structure-sensitive and that very small particles have low activity.[22b,44] After calcination at 750 °*C*, the loss of activity can be associated with the heavy sintering of the copper phase and the destruction of the mesostructure. As compared to the catalyst calcined at 550 °*C*, the one calcined at 650 °*C* (A-CuGaSi-650) showed somewhat lower selectivity levels. This may be ascribed to the formation of too large particles. Yet this was compensated by a higher conversion, attributed to the further migration of Cu, resulting in higher surface concentration. Overall, this one-pot catalyst achieved a high MeOH productivity (486 $\mu mol_{MeOH} g_{cat}^{-1} h^{-1}$ at 280 °*C*), almost reaching the productivity of the impregnated one. Like all catalysts discussed here, the activity levels appeared stable at each investigated temperature for a 5 *h* time on stream (see Figure S7).

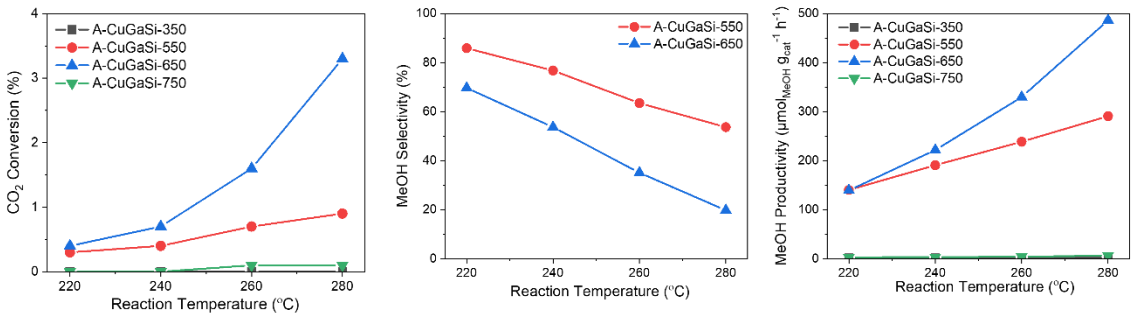


Figure 7. CO_2 conversion (left), MeOH selectivity (middle) and MeOH productivity (right) of A-CuGaSi catalysts as a function of the reaction temperature.

Conclusions

We show that a simple, direct, and continuous synthesis approach relying on the aerosol-assisted sol-gel process can be utilized to prepare highly efficient Cu-based catalysts for the hydrogenation of CO_2 to methanol. The process leads to spherical and mesostructured silica-based microparticles with highly dispersed Ga or Zn species and open mesopores. Copper can either be impregnated onto these doped supports or directly incorporated in the precursor solution, so that the catalyst is formed in one step. Similar performances can be reached even if the catalyst prepared by impregnation remained slightly more active than the one-step-made catalyst. Using a direct one-step method, however, decreases the environmental footprint of the synthesis process as compared to classical multi-step approaches. While Cu-SiO_2 formulations show very low activity, the addition of Ga or Zn in the silica matrix boosts both CO_2 conversion and methanol selectivity. This strong promotion effect is consistent with the proposition that Ga and Zn dopants favour the formation of active sites that are intrinsically more active for methanol synthesis (lower energy of activation) and less active for CO synthesis (higher energy of activation). While this one-step AASG method leads to the incorporation of Cu species dispersed into the walls of the metallosilicate materials, we show that calcination provokes their migration towards the catalyst surface and a progressive sintering of CuO nanoparticles. The optimized Ga-promoted catalysts had a methanol productivity as high as 0.5 *mmol* of methanol produced per *g* of catalyst and per *hour* at 280 *°C*.

Experimental

Catalyst preparation

SiO_2, Ga-SiO_2, and Zn-SiO_2 supports prepared by aerosol-assisted sol-gel

SiO_2, Ga-SiO_2, and Zn-SiO_2 supports were synthesized by the aerosol-assisted sol-gel (AASG) method.[33a] Solution A (45 *g* of ethanol (VWR, > 99.8 %), 8 *g* of distilled water, 3.88 *g* of Pluronic F127 (Sigma Aldrich) and solution B (12 *g* of TEOS (TCI Chemicals, > 97.0 %), 20 *g* of aqueous solution of HCl (Roth, 37 %) pH 2) were prepared and stirred overnight then mixed together. For the promoted supports, the nitrate salt of the doping element ($Ga(NO_3)_2.H_2O$ (Roth, 99.9995 %) or $Zn(NO_3)_2.H_2O$ (Roth, >99 %)) was added to the precursors solution to reach a Ga/Si or Zn/Si molar ratio of 0.05. The solution is then sprayed

with an atomizer from TSI with an air pressure of 30 *psi*. The aerosol goes through a tubular quartz tube heated at 450 °*C*. The dried powder is collected on a nitrocellulose filter (Sartorius Stedim, 0.45 *µm*). Powders are calcined in a muffle furnace under static air, first at 350 °*C* (1°C/min) for three hours, and then at 550 °*C* (1 °*C/min*) for three more hours. These materials are denoted Si-550, GaSi-550 and ZnSi-550.

Cu impregnation on preformed supports

A dry impregnation (DI) protocol was applied, using $Cu(NO_3)_2$ x 2.5 H_2O (Alfa Aesar, 98 %), to obtain a final copper loading of 10 *wt%*. The amount of impregnation solution (and its concentration) was determined from the measured pore volume. Prior to the impregnation, supports were ground with a mortar and a rammer. Then the copper solution was mixed with the ground support to obtain a homogeneous dough. A first drying step (50 °*C*, 1 *h*, static air) was applied before grinding the powder again and then a second drying step (90 °*C*, 1 *h*, static air) was applied. Powders were finally calcined at 350 °*C* (1 °*C/min*) under static air for three hours. The catalysts are denoted DI-Cu/Si-550, DI-Cu/GaSi-550 and DI-Cu/ZnSi-550.

One-pot preparation of Cu-(Ga)-(Zn)-SiO_2 by aerosol

The AASG protocol described above for the supports was simply modified by the addition of the copper precursor right before spray drying. $Cu(NO_3)_2.2.5H_2O$ (Alfa Aesar, 98 %) was added to the precursors solution to obtain a nominal Cu loading of 10 *wt.%*. For the Ga-promoted catalysts, various temperatures were tested for the last calcination step. Catalysts are denoted A-CuSi-X, A-CuGaSi-X or A-CuZnSi-X, where X represents the temperature of the last calcination step (350, 550, 650, or 750 °*C*).

Characterization

Textural properties were measured by N_2-physisorption at -196 °*C* using a Micrometrics Tristar 3000 instrument. Calcined samples were degassed overnight under vacuum at 150 °*C* prior to analysis. The BET model was used to determine specific surface area (SSA) under the relative pressure range of 0.05-0.30. Total pore volume (V_p) was estimated from the adsorption branch of the isotherm at $P/P_0 = 0.98$ and the average pore diameter (D_p) was estimated from

the BJH model applied on the adsorption isotherms. The microporous volume (V_{micro}) was estimated from the t-plot.

X-ray diffraction analyses was performed using a Bruker D8 Advance diffractometer (Bragg-Brentano geometry). The x-ray source operates at 1200 W (30 *mA*, 40 *kV*). Analyses are made at room temperature via the $K\alpha_{1,2}$ radiation of Cu ($\lambda = 0{,}15418$ *nm*) within a 2θ range of 5 ° and 80 ° with a step size of 0.02 ° (2θ) and 0.15 second per step. The detector was a Bruker Lynxeye XE-T. Some analyses were performed *in-situ* under air between 350 °*C* and 750 °*C* with a step size of 50 °*C*. The reactor chamber was an Anton Paar XRK 900. The height of the sample was adjusted each measurement to not skew the results. Identification of the phases was carried out using PFD-2 database and COD database.

XPS analyses were carried out on an SSX 100/206 photoelectrons spectrometer from Surface Science Instruments (USA) equipped with an Al RX monochromatic and micro-focused source (20 *mA*, 10 *kV*). Samples were disposed on a conducting carousel sample carrier made of aluminium thanks to double-sided adhesive tape. The pressure inside the analysis chamber is about 10^{-6} *Pa*. The angle between the normal to the surface and the axis of the input lens of the analyzer was 55 °. The analysed zone was approximately 1.4 mm^2 and the pass energy was fixed at 150 *eV*. Under these conditions, the half-height width (FWHM) of the Au $4f_{7/2}$ photo-peak measured on a standard cleaned gold sample was about 1.6 *eV*. An electron gun set at 8 *eV* and a nickel grid placed 3 *mm* above the surface of the sample were used to stabilize the charge. The C-(C,H) component of the C1s peak of carbon was set at 284.8 *eV* to set the scale of the binding energy. Data processing was carried out with the CasaXPS program (Casa Software Ltd, UK). The molar fractions were calculated using standard peak areas based on the acquisition parameters and sensitivity factors provided by the manufacturer.

ICP-AES analyses were performed on an ICP Thermo Scientific 6500 instrument after dissolution of the samples by sodium peroxide fusion.

SEM images have been obtained by a JEOL 7600F microscope under 10 *kV* or 15 *kV*. The emission current was about 100 μA. Prior scanning, samples were disposed on a carbon paper on an aluminium beak and were coated by gold or chromium under vacuum via Cressington Sputter Metal 208 HR instrument.

TEM images were obtained with a FEI Tecnai 120 Twin microscope, operating at 120 *kV* and equipped with a GatanOrius CCD numeric camera. The samples were prepared by ultrasonic dispersion of the powders in ethanol and a droplet of the dispersion was then placed on a carbon coated copper grid.

Cu dispersion was obtained by N_2O chemisorption using a Quantachrome ChemBET-3000 unit. The catalyst (*ca.* 100 *mg*) was first reduced in a fixed bed reactor under a 10 *vol.%* H_2/Ar mixture (Air Liquide 99.999 *%*, 20 *mL/min*, 5 *°C/min*) at 300 *°C* for 1 *h*, before being cooled to 30 *°C*. Then, the H_2/Ar flow was switched to 1 *vol.%* N_2O/Ar (20 *mL/min*). At this temperature, N_2O reacts selectively with the surface Cu atoms, with negligible bulk oxidation.[45] After 15 *min* under N_2O/Ar, the flow was switched to 10 *vol.%* H_2/Ar and the sample was reduced under the same conditions used the first time (300 *°C*, heating rate 5 *°C* min^{-1}). The consumption of H_2 was monitored using a thermal conductivity detector (TCD). The integration of this second reduction curve allowed calculation of the concentration of Cu atoms located at the surface. The TCD was calibrated with different amounts of pure CuO. Dispersion was defined as the ratio between surface Cu atoms and the total Cu atoms in the catalyst. The amount of copper atoms on the surface was calculated assuming a molar stoichiometry of N_2O/Cu = 0.5. An experimental error of ~10 *%* in relative has to be taken into account.

CO_2 Hydrogenation to methanol

Catalytic tests were performed in a fixed bed reactor. The catalyst was pressed, ground, and sieved in the 150 to 380 *µm* range, and then loaded on quartz wool in a stainless steel tubular reactor. Prior to the analyses, samples were reduced in the reactor under 30 *mL/min* of H_2 (Air Liquide, 99.999 *%*) for one hour at 300 *°C* (2 *°C/min*). After reduction, the system is pressurized (800 *kPa*) and fed by the gas mixture (20 *mL/min* of CO_2 and 5 *mL/min* of H_2) (Air Liquide, 99.999 *%*). Analyses are made at 280, 260, 240 and 220 *°C*. To check for an eventual deactivation of the catalyst, a supplementary measurement is done after a comeback at 280 *°C* (2 *°C/min*) at the end of the analysis. Each temperature is maintained for about five hours to ensure the steady state of the system. The exit gases are separated and analysed via a GC Perkin Elmer Autosystem XL instrument equipped with a Porapak Q column connected to a TCD and FID. The FID is equipped with a methanizer to quantify more accurately carbon oxides.

Acknowledgements

F.R.S.–F.N.R.S. is thanked for the acquisition of the *in situ* XRD equipment (project EQP UN00616F). Damien Debecker thanks the Francqui Foundation for the “Francqui Research Professor” chair.

References

[1] A. L. Burrell, J. P. Evans, M. G. De Kauwe, *Nat. Commun.* **2020**, *11*, 3853.

[2] J. Rogelj, D. Huppmann, V. Krey, K. Riahi, L. Clarke, M. Gidden, Z. Nicholls, M. Meinshausen, *Nature* **2019**, *573*, 357-363.

[3] M. Carmo, D. Stolten, in *Science and Engineering of Hydrogen-Based Energy Technologies* (Ed.: P. E. V. de Miranda), Academic Press, **2019**, pp. 165-199.

[4] (a) A. J. Hunt, E. H. K. Sin, R. Marriott, J. H. Clark, *ChemSusChem* **2010**, *3*, 306-322; (b) P. Melo, D. P. Debecker, *Waste Disposal & Sustainable Energy* **2019**, *1*, 53–65; (c) J. A. Martens, A. Bogaerts, N. De Kimpe, P. A. Jacobs, G. B. Marin, K. Rabaey, M. Saeys, S. Verhelst, *ChemSusChem* **2017**, *10*, 1039-1055.

[5] (a) B. Rego de Vasconcelos, J.-M. Lavoie, *Front. Chem.* **2019**, *7*, 392; (b) Z. Chehade, C. Mansilla, P. Lucchese, S. Hilliard, J. Proost, *Int. J. Hydrogen Energy* **2019**, *44*, 27637-27655; (c) G. Prieto, *ChemSusChem* **2017**, *10*, 1056-1070.

[6] (a) Y. Zhang, Y.-L. Zheng, H. Liu, *ChemSusChem (in press)* **2020**, https://doi.org/10.1002/cssc.202001290; (b) A. Kim, D. P. Debecker, F. Devred, V. Dubois, C. Sanchez, C. Sassoye, *Appl. Catal. B* **2018**, *220*, 615-625.

[7] X.-L. Du, Z. Jiang, D. S. Su, J.-Q. Wang, *ChemSusChem* **2016**, *9*, 322-332.

[8] (a) R. Kajaste, M. Hurme, P. Oinas, *AIMS Energy* **2018**, *6*, 1074-1102; (b) K. Räuchle, L. Plass, H.-J. Wernicke, M. Bertau, *Energy Technol.* **2016**, *4*, 193-200; (c) M. Bertau, H. Offermanns, L. Plass, F. Schmidt, H.-J. Wernicke, (Eds.), *Methanol: The Basic Chemical and Energy Feedstock of the Future*, Springer-Verlag Berlin Heidelberg, **2014**.

[9] M. Bowker, *ChemCatChem* **2019**, *11*, 4238-4246.

[10] J. Y. C. P. S. T. Campbell, *Catal. Lett.* **1995**, *31*, 313-324.

[11] J. Wu, M. Saito, M. Takeuchi, T. Watanabe, *Appl. Catal. A* **2001**, *218*, 235-240.

[12] (a) J. B. H. a. P. E. H. Nielsen, in *Handbook of Heterogeneous Catalysis,*, 2nd ed. (Ed.: H. K. G. Ertl, F. Schüth and J. Weitkamp), Wiley-VCH Verlag GmbH & Co. KGaA, Weinheim, Germany, **2008**; (b) S. Dang, H. Yang, P. Gao, H. Wang, X. Li, W. Wei, Y. Sun, *Catal. Today* **2019**, *330*, 61-75; (c) R. Guil-Lopez, N. Mota, J. Llorente, E. Millán, B. Pawelec, J. L. G. Fierro, R. Navarro, *Materials* **2019**, *12*, 3902.

[13] (a) R. Guil-López, N. Mota, J. Llorente, E. Millán, B. Pawelec, J. L. G. Fierro, R. M. Navarro, *Materials* **2019**, *12*, 3902; (b) M. Zabilskiy, V. L. Sushkevich, D. Palagin, M. A. Newton, F. Krumeich, J. A. van Bokhoven, *Nat. Commun.* **2020**, *11*, 2409.

[14] (a) F. Arena, G. Italiano, K. Barbera, S. Bordiga, G. Bonura, L. Spadaro, F. Frusteri, *Appl. Catal. A* **2008**, *350*, 16-23; (b) M. Behrens, F. Studt, I. Kasatkin, S. Kühl, M. Hävecker, F. Abild-Pedersen, S. Zander, F. Girgsdies, P. Kurr, B.-L. Kniep, M. Tovar, R. Fischer, J. Nørskov, R. Schlögl, *Science (New York, N.Y.)* **2012**, *336*, 893-897.

[15] (a) R. G. Herman, K. Klier, G. W. Simmons, B. P. Finn, J. B. Bulko, T. P. Kobylinski, *J. Catal.* **1979**, *56*, 407-429; (b) S. Mehta, G. W. Simmons, K. Klier, R. G. Herman, *J. Catal.* **1979**, *57*, 339-360.

[16] M. S. Spencer, *Catal. Lett.* **1990**, *60*, 55-60.

[17] (a) J. Schumann, M. Eichelbaum, T. Lunkenbein, N. Thomas, M. C. Álvarez Galván, R. Schlögl, M. Behrens, *ACS Catal.* **2015**, *5*, 3260-3270; (b) J. Toyir, P. R. r. de la Piscina, J. L. G. Fierro, N. s. Homs, *Appl. Catal B* **2001**, *29*, 207-215; (c) M.-J. Li, Z. Zeng, F. Liao, X. Hong, S. Tsang, *J. Catal.* **2016**, *343*, 157-167; (d) M. Saito, T. Fujitani, I. Takahara, T. Watanabe, M. Takeuchi, Y. Kanai, K. Moriya, T. Kakumoto, *Energy Convers. Manage.* **1995**, *36*, 577-580.

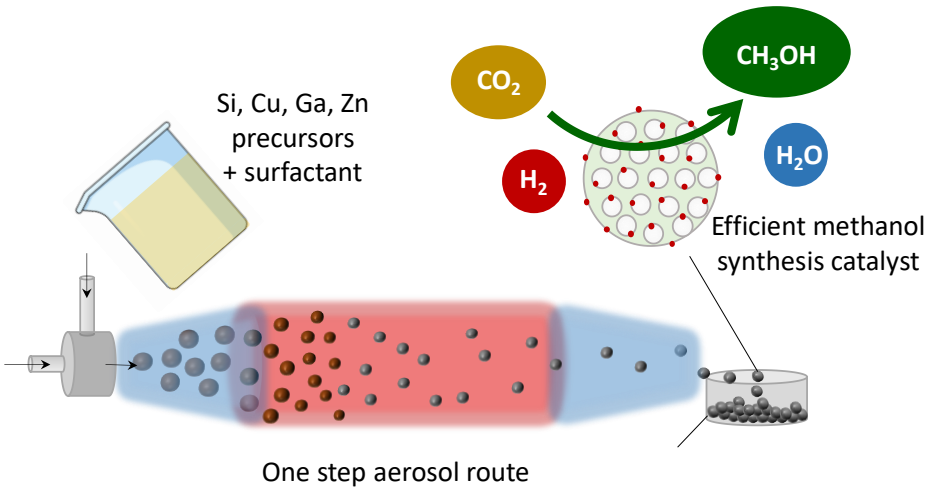
[18] (a) P. B. Sanguineti, M. A. Baltanás, A. L. Bonivardi, *Appl. Catal. A* **2015**, *504*, 476-481; (b) X.-M. Liu, G. Q. Lu, Z.-F. Yan, *Appl. Catal. A* **2005**, *279*, 241-245.

[19] (a) S. Natesakhawat, J. W. Lekse, J. P. Baltrus, P. R. Ohodnicki, B. H. Howard, X. Deng, C. Matranga, *ACS Catal.* **2012**, *2*, 1667-1676; (b) R. Ladera, F. J. Pérez-Alonso, J. M. González-Carballo, M. Ojeda, S. Rojas, J. L. G. Fierro, *Appl. Catal. B* **2013**, *142-143*, 241-248.

[20] J. C. Medina, M. Figueroa, R. Manrique, J. Rodríguez Pereira, P. D. Srinivasan, J. J. Bravo-Suárez, V. G. Baldovino Medrano, R. Jiménez, A. Karelovic, *Catal. Sci. Technol.* **2017**, *7*, 3375-3387.
[21] E. Lam, G. Noh, K. W. Chan, K. Larmier, D. Lebedev, K. Searles, P. Wolf, O. V. Safonova, C. Copéret, *Chem. Sci.* **2020**, *11*, 7593-7598.
[22] (a) A. Karelovic, P. Ruiz, *Catal. Sci. Technol.* **2015**, *5*, 869-881; (b) A. Karelovic, G. Galdames, J. C. Medina, C. Yévenes, Y. Barra, R. Jiménez, *J. Catal.* **2019**, *369*, 415-426.
[23] (a) S. Kuld, M. Thorhauge, H. Falsig, C. F. Elkjær, S. Helveg, I. Chorkendorff, J. Sehested, *Science* **2016**, *352*, 969-974; (b) K. Chen, H. Fang, S. Wu, X. Liu, J. Zheng, S. Zhou, X. Duan, Y. Zhuang, S. Chi Edman Tsang, Y. Yuan, *Appl. Catal. B* **2019**, *251*, 119-129; (c) S. Tada, S. Kayamori, T. Honma, H. Kamei, A. Nariyuki, K. Kon, T. Toyao, K.-i. Shimizu, S. Satokawa, *ACS Catal.* **2018**, *8*, 7809-7819.
[24] (a) X. Dong, F. Li, N. Zhao, F. Xiao, J. Wang, Y. Tan, *Appl. Catal. B* **2016**, *191*, 8-17; (b) D. Allam, S. Bennici, L. Limousy, S. Hocine, *C. R. Chim.* **2019**, *22*, 227-237; (c) X. Fang, Y. Men, F. Wu, Q. Zhao, R. Singh, P. Xiao, T. Du, P. A. Webley, *J. CO2 Utilization* **2019**, *29*, 57-64; (d) A. Karelovic, A. Bargibant, C. Fernández, P. Ruiz, *Catal. Today* **2012**, *197*, 109-118.
[25] D. P. Debecker, S. Le Bras, C. Boissiere, A. Chaumonnot, C. Sanchez, *Chem. Soc. Rev.* **2018**, *47*, 4112-4155.
[26] C. Boissiere, D. Grosso, A. Chaumonnot, L. Nicole, C. Sanchez, *Adv. Mater.* **2011**, *23*, 599-623.
[27] C. Niu, M. Liu, X. Gao, X. Ye, Y. Wen, Y. Liu, X. Wang, *ACS Omega* **2019**, *4*, 4397-4404.
[28] (a) L. Kuai, J. Wang, T. Ming, C. Fang, Z. Sun, B. Geng, J. Wang, *Sci. Rep.* **2015**, *5*, 9923; (b) D. P. Debecker, *Chem. Record* **2018**, *18*, 662-675.
[29] (a) A. B. D. Nandiyanto, K. Okuyama, *Adv. Powder Technol.* **2011**, *22*, 1-19; (b) V. Smeets, W. Baaziz, O. Ersen, E. M. Gaigneaux, C. Boissière, C. Sanchez, D. P. Debecker, *Chem. Sci.* **2020**, *11*, 954-961.
[30] V. Smeets, C. Boissière, C. Sanchez, E. M. Gaigneaux, E. Peeters, B. F. Sels, M. Dusselier, D. P. Debecker, *Chem. Mater.* **2019**, *31*, 1610-1619.
[31] S. Pega, C. Boissière, D. Grosso, T. Azaïs, A. Chaumonnot, C. Sanchez, *Angew. Chem. Int. Ed.* **2009**, *48*, 2784-2787.
[32] (a) N. Godard, A. Vivian, L. Fusaro, L. Cannavicci, C. Aprile, D. P. Debecker, *ChemCatChem* **2017**, *9*, 2211-2218; (b) A. Vivian, L. Fusaro, D. P. Debecker, C. Aprile, *ACS Sus. Chem. Eng.* **2018**, *6*, 14095–14103.
[33] (a) D. P. Debecker, M. Stoyanova, F. Colbeau-Justin, U. Rodemerck, C. Boissière, E. M. Gaigneaux, C. Sanchez, *Angew. Chem. Int. Ed.* **2012**, *51*, 2129-2131; (b) D. P. Debecker, M. Stoyanova, U. Rodemerck, F. Colbeau-Justin, C. Boissère, A. Chaumonnot, A. Bonduelle, C. Sanchez, *Appl. Catal. A* **2014**, *470*, 458-466; (c) S. Maksasithorn, P. Praserthdam, K. Suriye, D. P. Debecker, *Microporous Mesoporous Mater.* **2015**, *213*, 125-133.
[34] M. T. Le, J. Craenenbroeck, I. Van Driessche, S. Hoste, *Appl. Catal. A* **2003**, *249*, 355-364.
[35] S. Ramesh, K. Indukuri, O. Riant, D. P. Debecker, *Org. Proc. Res. Dev.* **2018**, *22*, 1846-1851.
[36] A. Sachse, V. Hulea, K. L. Kostov, N. Marcotte, M. Y. Boltoeva, E. Belamie, B. Alonso, *Chem. Commun.* **2012**, *48*, 10648-10650.
[37] M. Faustini, M. Giraud, D. Jones, J. Rozière, M. Dupont, T. R. Porter, S. Nowak, M. Bahri, O. Ersen, C. Sanchez, C. Boissière, C. Tard, J. Peron, *Adv. Energy Mater.* **2019**, *9*, 1802136.
[38] A. Kim, C. Sanchez, B. Haye, C. Boissiere, C. Sassoye, D. Debecker, *ACS Appl. Nano Mater.* **2019**, *2*, 3220–3230.
[39] J. M. Thomas, *Angew. Chem. Int. Ed.* **2009**, *48*, 3390-3391.
[40] E. Lam, J. J. Corral-Pérez, K. Larmier, G. Noh, P. Wolf, A. Comas-Vives, A. Urakawa, C. Copéret, *Angew. Chem. Int. Ed.* **2019**, *58*, 13989-13996.
[41] M. Behrens, *Recycl. Catal.* **2015**, *2*, 78-86.
[42] J. C. Groen, L. A. A. Peffer, J. Pérez-Ramírez, *Microporous Mesoporous Mater.* **2003**, *60*, 1-17.
[43] (a) I. C. f. D. Data, **2010**; (b) H.-Q. Wu, X.-W. Wei, M.-W. Shao, J.-S. Gu, M.-Z. Qu, *Chem. Phys. Lett.* **2002**, *364*, 152-156.

[44] R. van den Berg, G. Prieto, G. Korpershoek, L. I. van der Wal, A. J. van Bunningen, S. Lægsgaard-Jørgensen, P. E. de Jongh, K. P. de Jong, *Nat. Commun.* **2016**, *7*, 13057.
[45] S. Sato, R. Takahashi, T. Sodesawa, K.-i. Yuma, Y. Obata, *J. Catal.* **2000**, *196*, 195-199.

Graphical abstract



TOC

Ga- and Zn-doped Cu-based hydrogenation catalysts are prepared in one step via aerosol-assisted sol-gel chemistry; they reach good performance in the CO_2 to methanol reaction. The synthesis method is direct, simple, continuous, and scalable. It leads to high-surface area mesoporous catalysts with the dopant dispersed in the silica matrix and copper nanoparticles at the catalyst surface.

CO_2 hydrogenation to methanol with Ga- and Zn-doped mesoporous Cu/SiO_2 catalysts prepared by the aerosol-assisted sol-gel process

Charlie Paris,[a,#] Dr. Alejandro Karelovic,[b,*] Raydel Manrique,[b] Dr. Solène Le Bras,[a] Dr. François Devred,[a] Dr. Vit Vykoukal,[c] Dr. Ales Styskalik,[c,d] Pierre Eloy,[a] Prof. Damien P. Debecker[a]*

[a] Institute of Condensed Matter and Nanoscience (IMCN), Université catholique de Louvain (UCLouvain), Place Louis Pasteur, 1, box L4.01.09, 1348 Louvain-La-Neuve, Belgium.

[b] Carbon and Catalysis (CarboCat), Department of Chemical Engineering, Faculty of Engineering, University of Concepcion, Chile.

[c] Masaryk University, Department of Chemistry, Kotlarska 2, CZ-61137 Brno, Czech Republic

[d] Masaryk University, CEITEC MU, Kamenice 5, CZ-62500 Brno, Czech Republic

* corresponding authors: akarelov@udec.cl, damien.debecker@uclouvain.be

[#] currently at Cardiff Catalysis Institute (CCI), School of Chemistry, Cardiff University, Main Building, Park Place, Cardiff, CF10 3AT, UK. E-mail: pariscb@cardiff.ac.uk

Electronic Supporting Information

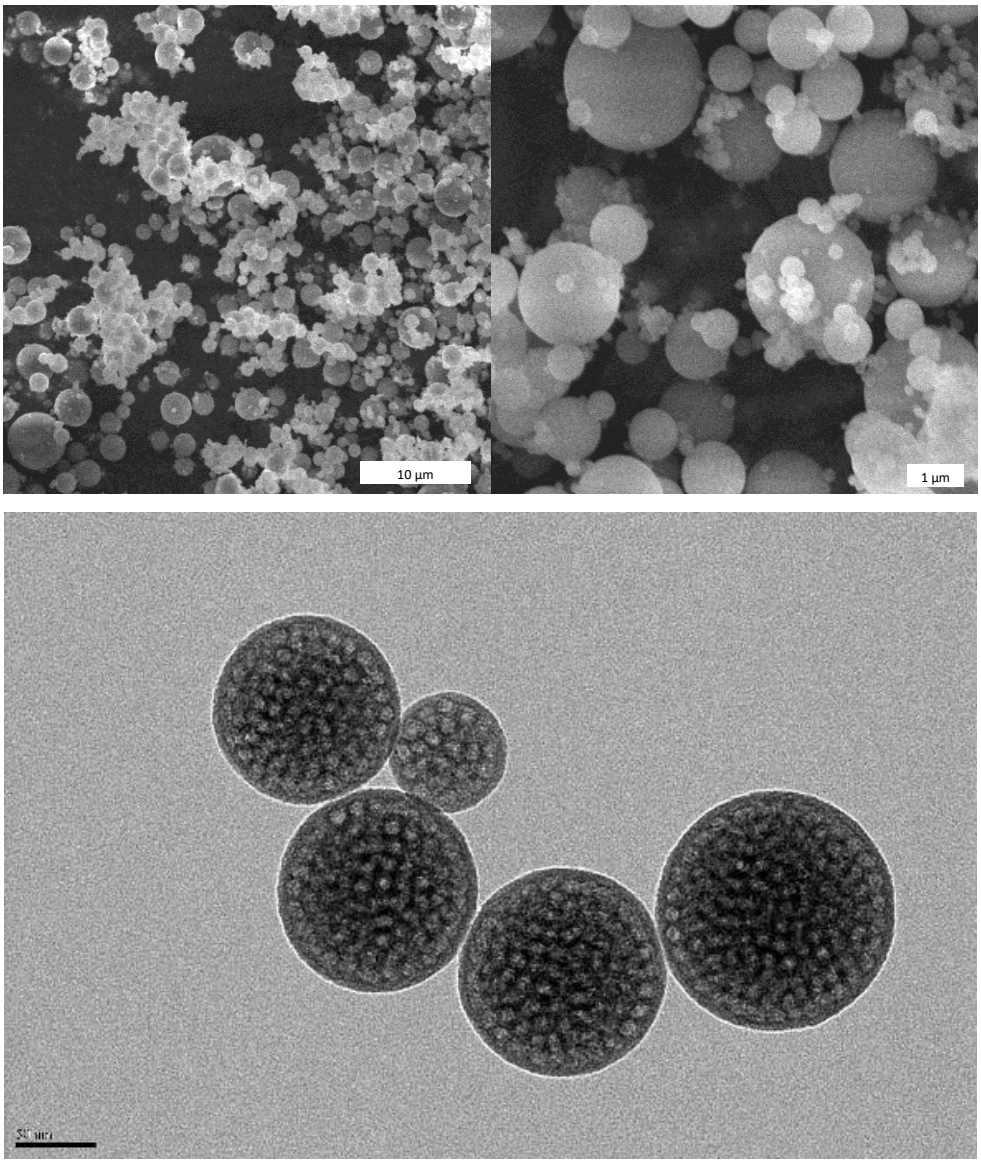


Figure S1. Mesoporous silica support prepared by the aerosol-assisted sol-gel process (Si-550) as observed in (top) SEM and (bottom) TEM.

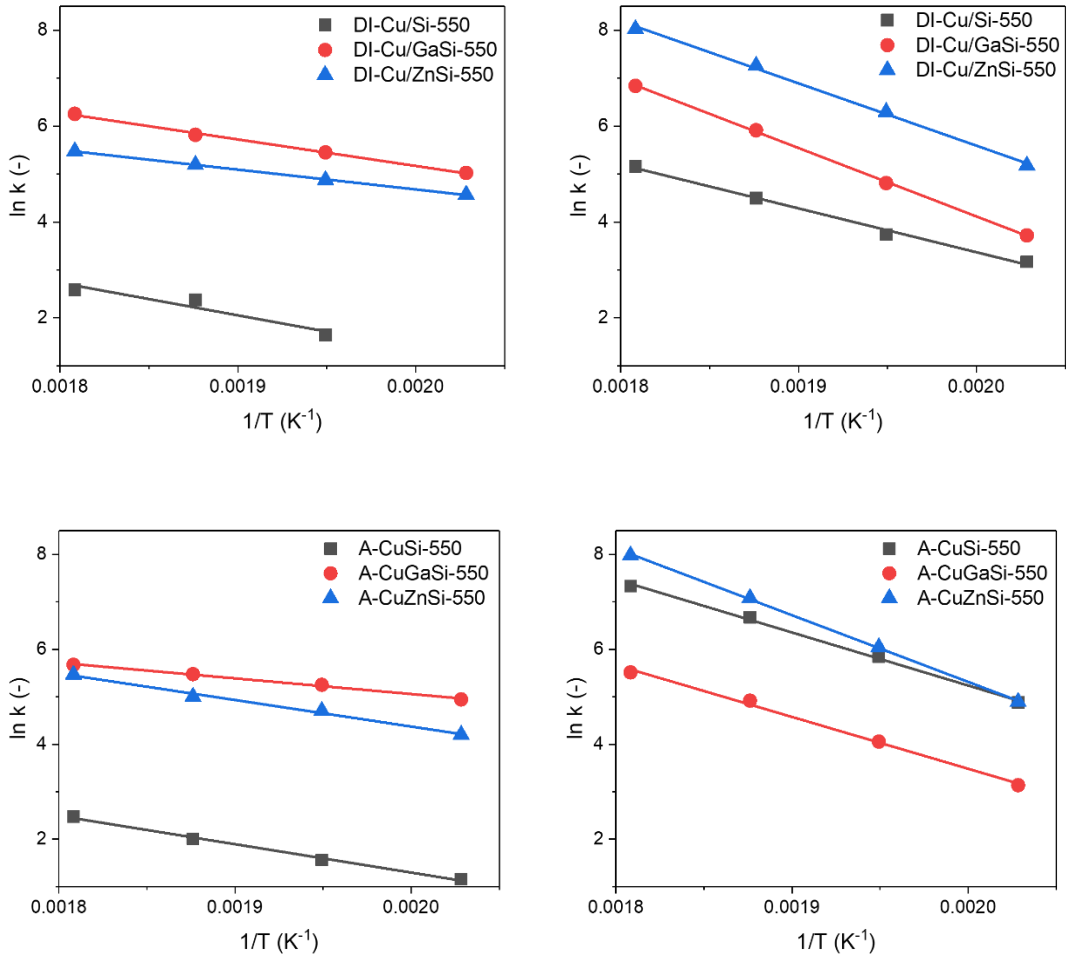


Figure S2. Arrhenius plots for determination of activation energy of methanol (left) and CO (right) synthesis for catalysts calcined at 550 ºC and prepared by impregnation (top) or aerosol (bottom).

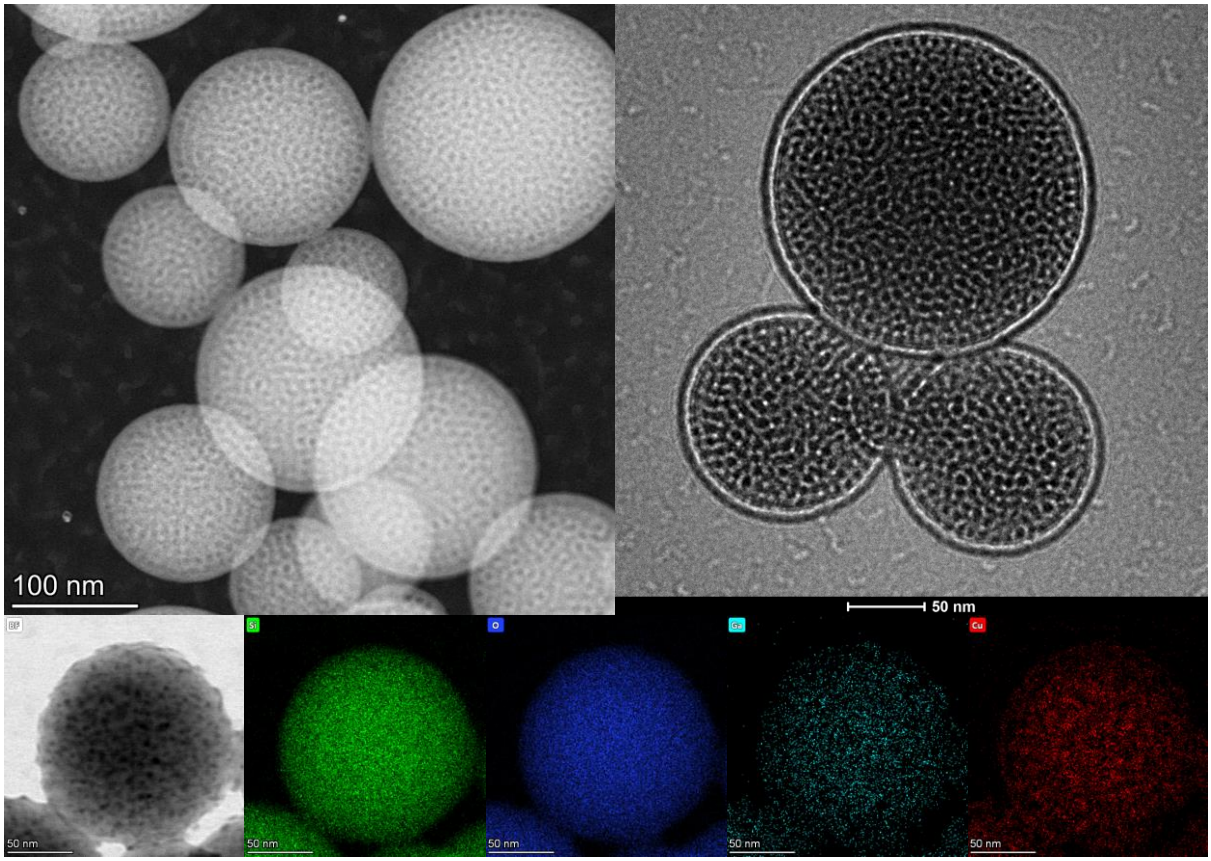


Figure S3. Electron micrographs of A-CuGaSi-550 observed in (top left) dark field STEM, (top right) TEM, and (bottom) STEM-EDS with elemental mapping of Si in green, O in blue, Ga in indigo, Cu in red.

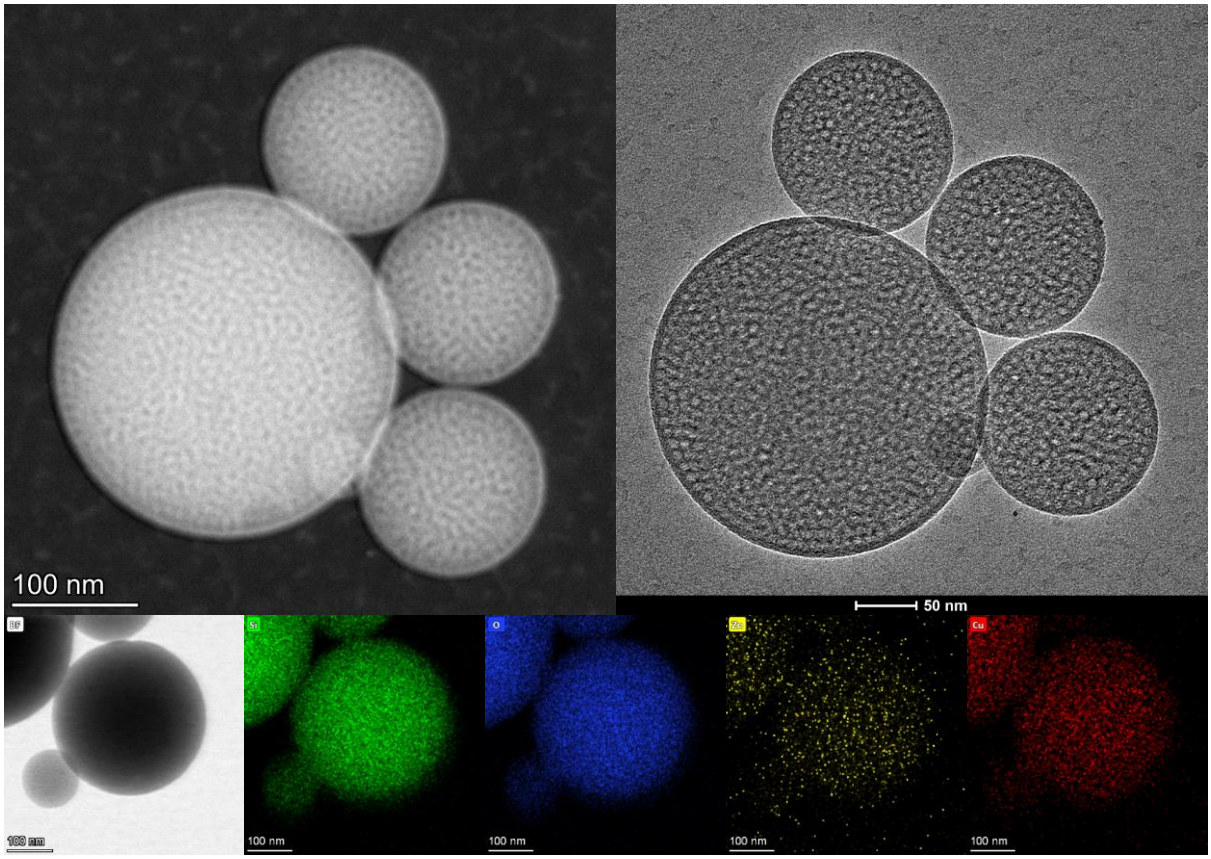


Figure S4. Electron micrographs of A-CuZnSi-550 observed in (top left) dark field STEM, (top right) TEM, and (bottom) STEM-EDS with elemental mapping of Si in green, O in blue, Zn in yellow, Cu in red.

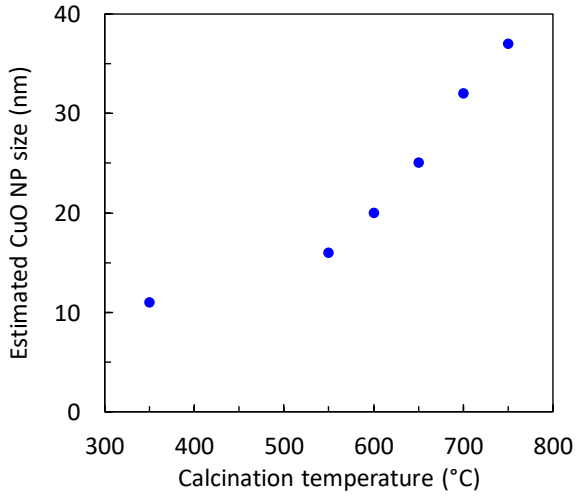


Figure S5. CuO nanoparticles size (determined via the Scherrer equation) as a function of the applied temperature for A-CuSi.

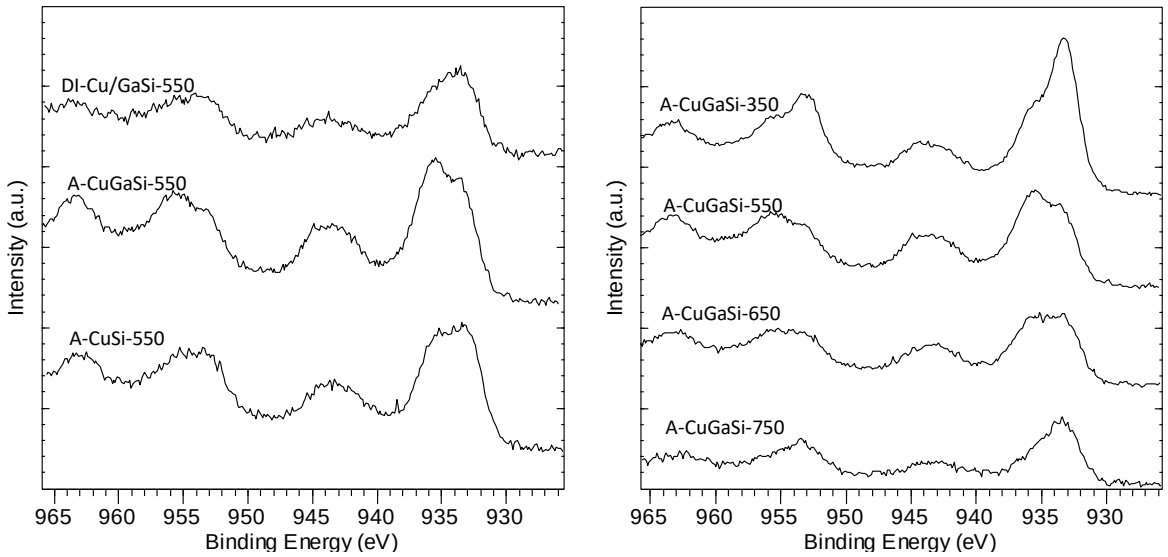


Figure S6. XPS Cu 2p peak. The Cu $2p_{3/2}$ is large (932-936 eV) and accompanied by a shake-up satellite peak (943 eV) that accounts for a little less than 50% of the main peak. This corresponds to Cu^{2+} species as typically found in CuO (consistent with XRD data) [Biesinger, Surf. Interface Anal. 2017, 49, 1325]. This interpretation particularly valid for the catalyst that do not contain Ga and for those where the interaction between Cu and Ga is probably weak (the one prepared by DI and the one calcined at 750°C, where a complete sintering of CuO is observed). On the contrary, for the sample where a strong interaction between the Cu and the Ga can be expected (A-CuGaSi-550 and A-CuGaSi-650, which are also the most active catalysts), the main peak appears larger, with a stronger contribution at higher BE. It is suggested that this broadening could be associated with the interaction between Ga and Cu. The nature of this interaction is however unclear. The proportion of the satellite peak remains stable, indicating the presence of Cu^{2+} species. Note that the catalyst calcined at 350°C only displays a peculiar Cu $2p_{3/2}$ peak (with a smaller satellite peak and a sharper contribution at 934 eV), possibly associated with the presence of some reduced Cu species (Cu^{+} species do not lead to the formation of a satellite peak).

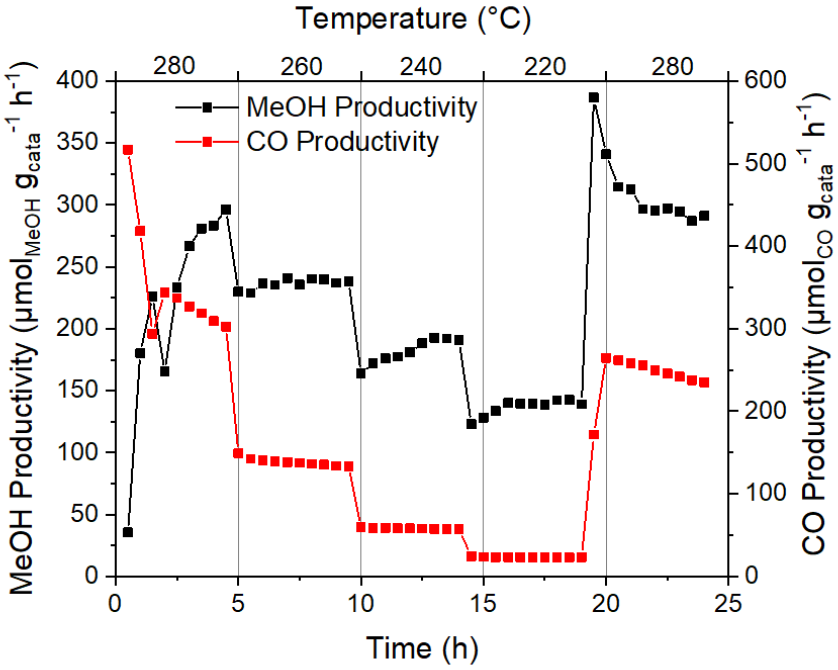


Figure S7. Productivity, as a function of time, towards MeOH (black) and CO (red) of A-CuGaSi-650. Each temperature (280, 260, 240, and 220°C) is maintained for about 5 hours. The measurement at 280°C performed as the first step was repeated at the end of the testing procedure and showed similar levels of MeOH and CO productivity, suggesting that no marked deactivation phenomenon occurs in the conditions used here.

Table S1. Activation energies of both methanol and CO synthesis for catalysts calcined at 550°C and prepared by dry impregnation or by one-pot AASG.

Catalyst	**Ea(MeOH) (kJ/mol)**	**Ea(CO) (kJ/mol)**
DI-Cu/Si-550	56	76
DI-Cu/GaSi-550	46	119
DI-Cu/ZnSi-550	34	108
A-CuSi-550	49	117
A-CuGaSi-550	27	91
A-CuZnSi-550	46	91